

# Monte Carlo Simulation of Carboxylic Acid Phase Equilibria

Scott Clifford,<sup>†</sup> Kim Bolton,<sup>‡</sup> and Deresh Ramjugernath<sup>\*,†</sup>

School of Chemical Engineering, University of KwaZulu-Natal, King George V Avenue, 4041, Durban, South Africa, and School of Engineering, University College of Borås, SE-50190, Borås, Sweden

Received: April 24, 2006; In Final Form: August 22, 2006

Configurational-bias Monte Carlo simulations were carried out in the Gibbs ensemble to generate phase equilibrium data for several carboxylic acids. Pure component coexistence densities and saturated vapor pressures were determined for acetic acid, propanoic acid, 2-methylpropanoic acid, and pentanoic acid, and binary vapor–liquid equilibrium (VLE) data for the propanoic acid + pentanoic acid and 2-methylpropanoic acid + pentanoic acid systems. The TraPPE-UA force field was used, as it has recently been extended to include parameters for carboxylic acids. To simulate the branched compound 2-methylpropanoic acid, certain minor assumptions were necessary regarding angle and torsion terms involving the  $-\text{CH}-$  pseudo-atom, since parameters for these terms do not exist in the TraPPE-UA force field. The pure component data showed good agreement with the available experimental data, particularly with regard to the saturated liquid densities (mean absolute errors were less than 1.1%). On average, the predicted critical temperature and density were within 1% of the experimental values. All of the binary simulations showed good agreement with the experimental  $x$ – $y$  data. However, the TraPPE-UA force field predicts saturated vapor pressures of pure components that are larger than the experimental values, and consequently the  $P$ – $x$ – $y$  and  $T$ – $x$ – $y$  data of the binary systems also deviate from the measured data.

## 1. Introduction

Carboxylic acids are commercially important chemicals and are involved in a number of industrially relevant separation processes. They are extremely useful as the basic building blocks of cleaning agents such as soaps and detergents because of their amphipathic properties.<sup>1,2</sup> Furthermore, these acids are necessary raw materials in the production of nylon, biodegradable plastics, and certain pharmaceuticals, they are used as buffers and acidulents (food preservatives), flavoring agents, fungicides, and insecticides, biomass products, and catalysts.<sup>1,3,4</sup> In addition, carboxylic acid derivatives include chemical species such as esters, acyl halides, acid anhydrides, nitriles, and amides<sup>2,5</sup> that find widespread application in various commercial sectors. Carboxylic acids also form stable oxidation products and, hence, are often present in aqueous waste streams and as byproducts of industrial operations.<sup>6</sup> To design and operate equipment for the removal, separation, and purification of the acids, accurate and reliable pure component and binary VLE data are essential. However, experimental data for these acids are rare<sup>7</sup> due to their aggressive and difficult chemical nature (the acids are strongly self- and cross-associating species in both the liquid and vapor phases<sup>8</sup>).

The use of configurational-bias Monte Carlo methods<sup>9–17</sup> in the Gibbs ensemble<sup>18–21</sup> (along with constant improvement in readily available computer hardware) has made computer simulation of complex systems viable. In addition, recent progress in the field of molecular simulation has led to the development of force fields capable of dealing with charged and associating compounds such as carboxylic acids.<sup>22</sup> Molecular simulation offers an ideal tool for obtaining VLE data in

an efficient and cost-effective manner,<sup>23,24</sup> and in the long-term it offers the possibility of replacing expensive laboratory measurements.

In this work we used the Gibbs ensemble Monte Carlo (GEMC) method with the force field developed by Kamath and co-workers<sup>22</sup> to calculate pure component saturated vapor pressure and density data for four carboxylic acids, namely, acetic acid, propanoic acid, 2-methylpropanoic acid, and pentanoic acid. This force field was also used to predict binary VLE data for the propanoic acid + pentanoic acid and 2-methylpropanoic acid + pentanoic acid systems. The simulation results are compared to experimental data measured by Clifford et al.<sup>7</sup> Although the pure component acetic acid and pentanoic acid systems have been studied previously,<sup>22</sup> this contribution presents the first simulations of pure propanoic acid and 2-methylpropanoic acid systems. In the latter case, the influence of branched hydrocarbon chains needed to be considered. This is also the first time that VLE for binary carboxylic acid systems have been obtained from simulations.

## 2. Methods

**2.1. Potential Model.** The TraPPE-UA force field,<sup>25–27</sup> with the improvements proposed by Kamath et al. for carboxylic acids,<sup>22</sup> was used in this work. The nonbonded (i.e., intermolecular) energy is calculated from the summation of pairwise Lennard–Jones (LJ) 12–6 and Coulombic interactions:<sup>22</sup>

$$U(r_{ij}) = 4\epsilon_{ij} \left[ \left( \frac{\sigma_{ij}}{r_{ij}} \right)^{12} - \left( \frac{\sigma_{ij}}{r_{ij}} \right)^6 \right] + \frac{q_i q_j}{4\pi\epsilon_0 r_{ij}} \quad (1)$$

where  $U$  is the intermolecular energy,  $r_{ij}$  the distance separating interaction sites  $i$  and  $j$ ,  $\epsilon_{ij}$  and  $\sigma_{ij}$  are the LJ well depth and size parameters, respectively, and  $q_i$  and  $q_j$  represent the partial charges of sites  $i$  and  $j$ . The parameters for like interactions

\* Corresponding author. E-mail: ramjuger@ukzn.ac.za.

<sup>†</sup> University of KwaZulu-Natal.

<sup>‡</sup> University College of Borås.

**TABLE 1: Parameters for Nonbonded Interactions**

pseudo-atom	$\epsilon_{ii}/k_B$ [K]	$\sigma_{ii}$ [Å]	$q_i$ [e]
C	41.0	3.90	0.42
O=C	79.0	3.05	-0.45
O-H	93.0	3.02	-0.46
H	0.0	0.00	0.37
CH <sub>3</sub> -(C=)	98.0	3.75	0.12
CH <sub>2</sub> -(C=)	46.0	3.95	0.12
(CH <sub>x</sub> )-CH <sub>2</sub> -(CH <sub>x</sub> )	46.0	3.95	0.0
CH <sub>3</sub> -(CH <sub>x</sub> )	98.0	3.75	0.0

**TABLE 2: Fixed Bond Lengths, Equilibrium Bond Angles ( $\theta_0$ ), and Bending Constants**

bond	length [Å]	bond	angle [°]	$k_\theta/k_B$ [K rad <sup>-2</sup> ]
C=O	1.214	C-O-H	107	17600
C-O	1.364	O=C-O	123	40300
C-CH <sub>x</sub>	1.520	CH <sub>x</sub> -C-O	111	35300
O-H	0.970	CH <sub>x</sub> -C=O	126	40300

(i.e.,  $\epsilon_{ii}$  and  $\sigma_{ii}$ ) are presented in Table 1, and the Lorentz–Berthelot mixing rules

$$\sigma_{ij} = \frac{\sigma_{ii} + \sigma_{jj}}{2}, \epsilon_{ij} = \sqrt{\epsilon_{ii}\epsilon_{jj}} \quad (2)$$

were used to determine the parameters for unlike interactions. Lennard–Jones interactions were truncated beyond an intermolecular distance of 14 Å, and standard long-range analytical tail corrections were applied.<sup>22</sup>

The TraPPE-UA model uses fixed bond lengths, and angle bending is described by a simple harmonic potential:<sup>22</sup>

$$U_{\text{bend}} = \frac{k_\theta}{2}(\theta - \theta_0)^2 \quad (3)$$

where  $\theta$  is the bond angle,  $\theta_0$  is the equilibrium angle, and  $k_\theta$  is the force constant. The values of the various bond lengths, angles, and force constants are listed in Table 2.

The torsional potentials used to determine the motion of the dihedral angles consisted of cosine series. For dihedral angles involving the carboxyl group, the following functional form is used. (In the original paper by Kamath et al.,<sup>22</sup> there is an error in the second term of eq 4, where their equation reads  $c_2[1 - \cos(2\phi)]$ . However, the correct form that was used in their work (and the work presented here) is  $c_2[1 - \cos^2\phi]$ .<sup>28</sup>)

$$U_{\text{torsion}} = c_1[1 + \cos(\phi + f_1)] + c_2[1 - \cos^2\phi] \quad (4)$$

while torsions of the alkane tail (for carboxylic acids of sufficient length) are described by eq 5:

$$U_{\text{torsion}} = \frac{V_1}{2}(1 + \cos\phi) + \frac{V_2}{2}(1 - \cos(2\phi)) + \frac{V_3}{2}(1 + \cos(3\phi)) \quad (5)$$

The values of the constants in eqs 4 and 5 are given in Table 3.

Since the studies of Kamath et al.<sup>22</sup> were restricted to linear carboxylic acids, the parameters for bond angles and torsions involving the -CH- functional group of 2-methylpropanoic acid are not available. In this work the CH-C=O and CH-C-O angle energies are described using the same parameters that are used for CH<sub>x</sub>-C=O and CH<sub>x</sub>-C-O ( $x = 2$  or  $3$ ).<sup>22</sup> Parameters for the CH<sub>3</sub>-CH-C=O, CH<sub>3</sub>-CH-C-O, and CH-C-O-H dihedral energies are assumed to be the same as those for the CH<sub>x</sub>-CH<sub>2</sub>-C=O, CH<sub>x</sub>-CH<sub>2</sub>-C-O, and CH<sub>x</sub>-C-O-H torsional energies. Hence, it is assumed that, in this

**TABLE 3: Torsional Potential Parameters**

dihedral	$c_1/k_B$ [K]	$c_2/k_B$ [K]	$f_1$ [°]
O=C-O-H	630.0	1562.4	180
CH <sub>x</sub> -C-O-H	630.0	1562.4	0
CH <sub>x</sub> -CH <sub>2</sub> -C=O	630.0	1562.4	180
CH <sub>x</sub> -CH-C=O	630.0	1562.4	180
	V1 [K]	V2 [K]	V3 [K]
CH <sub>x</sub> -CH <sub>2</sub> -C-O	710.06	-136.38	1582.64
CH <sub>x</sub> -CH-C-O	710.06	-136.38	1582.64
CH <sub>x</sub> -CH <sub>2</sub> -CH <sub>2</sub> -CH <sub>x</sub>	710.06	-136.38	1582.64

**TABLE 4: Probabilities of Performing Different Move Types**

move	probability	
	pure component	binary mixture
volume change	0.006	0.002
CBMC	0.194	0.198
AVBMC		0.050
molecule regrowth	0.267	0.250
molecule translation	0.266	0.250
molecule rotation	0.267	0.250

instance, the number of hydrogens attached to the  $\alpha$ -carbon does not effect the force field. The torsional parameters involving the -CH<sub>2</sub>- functional group were not listed in the original paper by Kamath et al.<sup>22</sup> and were taken from existing torsions, namely, O-C-O-H, CH<sub>x</sub>-CH<sub>2</sub>-CH<sub>2</sub>-CH<sub>x</sub>, and CH<sub>x</sub>-C-O-H, by Martin and Potoff.<sup>28</sup>

**2.2. Simulation Details.** Monte Carlo simulations in the Gibbs ensemble,<sup>18–21</sup> as implemented in the MCCCSTowhee source code,<sup>28</sup> were used to calculate the data presented here. The coupled–decoupled configurational-bias technique<sup>29</sup> was utilized to enhance the sampling of phase space. An inner cutoff radius of 10 Å was used for the intermolecular interactions following the dual-cutoff algorithm advanced by Vlught et al.,<sup>30</sup> which more than doubles the configurational-bias Monte Carlo (CBMC) computation speed.<sup>28</sup> The bias that is introduced is removed through corrections applied in the acceptance criteria. The aggregated volume bias (AVB) move, which was specifically developed for molecules such as carboxylic acids that associate strongly and tend to form clusters,<sup>31</sup> was included for the binary VLE simulations. Long-range electrostatic energy interactions were computed using an Ewald sum with tinfoil boundary conditions.<sup>22</sup> The maximum number of inverse space vectors,  $K_{\text{max}}$ , was set to 5 and  $\alpha$  was calculated by dividing  $\kappa L$  (set to 5.6) by the shortest box length.<sup>28,32</sup>

For the pure component simulations the NVT Gibbs ensemble was used, with 300, 250, 200, and 200 molecules for acetic, propanoic, 2-methylpropanoic, and pentanoic acids, respectively, and the NPT Gibbs ensemble was employed for binary simulations with the system size constrained to 300 molecules. This allowed statistically converged data to be calculated in a computationally feasible time. Increasing the number of molecules does not meaningfully alter the results presented here. Equilibration of the systems, as evidenced by constant average vapor and liquid densities, was obtained by running the simulations for between 1.5 and 5 million Monte Carlo steps. The production periods during which equilibrium data were recorded consisted of 3 to 6 million Monte Carlo steps. Each production cycle was divided into five blocks to allow the standard deviations of the ensemble averages to be calculated.<sup>33</sup> The fixed probabilities for the various types of moves in each simulation differed slightly for the pure and binary simulations and are listed in Table 4. The probability of performing CBMC particle moves was adjusted to obtain approximately one

**TABLE 5: Results for the Pure Component Carboxylic Acid Simulations**

compound	<i>T</i> [K]	<i>P</i> [kPa]	$\rho_{\text{liq}}$ [g/mL]	$\rho_{\text{vap}}$ [g/mL]
acetic acid	350	35.82	0.974	7.92E-04
	400	203.56	0.919	4.09E-03
	450	734.16	0.857	1.27E-02
	500	1744.83	0.778	3.10E-02
	550	3919.32	0.677	7.53E-02
propanoic acid	350	18.85	0.929	4.81E-04
	400	114.21	0.875	2.63E-03
	450	438.66	0.820	9.85E-03
	500	1092.60	0.736	2.34E-02
	550	2611.01	0.654	6.04E-02
2-methylpropanoic acid	350	11.14	0.884	3.45E-04
	400	69.06	0.834	1.98E-03
	450	306.76	0.774	8.09E-03
	500	897.15	0.710	2.25E-02
	550	2110.33	0.622	5.47E-02
pentanoic acid	400	28.28	0.841	9.06E-04
	450	168.81	0.791	4.97E-03
	500	460.26	0.731	1.25E-02
	550	1260.40	0.671	3.50E-02
	600	2354.99	0.571	7.24E-02

accepted molecule swap for every 10 Monte Carlo cycles. The fixed probabilities shown in Table 4 and the maximum volume, translation, and rotational displacements were selected so that an acceptance ratio of 50% was attained for each of these moves.

As discussed by McKnight et al.,<sup>34</sup> it is important to select initial volumes and numbers of molecules for these binary simulations that do not substantially differ from the final equilibrium values. However, it is also important that one does not initialize the system at a pre-supposed equilibrium and begin analysis before one has reached the true equilibrium. In addition, using Raoult's law to estimate the starting partial pressures, as suggested by McKnight and co-workers,<sup>34</sup> is not possible for the strongly associating, nonideal carboxylic acids studied here. Therefore, in this work experimental data<sup>7</sup> were used to estimate reasonable initial pressures. The combined volume of the two simulation boxes was adjusted so that approximately two-thirds of the molecules were in the liquid box. It is important to note that a substantial change in average VLE properties was observed in our simulations before data were collected, showing that the systems had equilibrated and that the results do not pertain to the initial conditions.

### 3. Results and Discussion

**3.1. Pure Component Simulations.** The simulated results for the pure component systems are given in Table 5, and the saturated vapor pressures and vapor–liquid coexistence data are shown in Figures 1–4. The vapor pressures are presented as Clausius–Clapeyron plots to allow the critical pressure and normal boiling point to be determined (discussed below). The average statistical standard deviations calculated from the block averages are less than 1.25% for the saturated liquid density and 8.5% for the saturated vapor density and pressure. Previous simulation results are available for acetic acid and pentanoic acid<sup>22</sup> and are included for comparison.

The saturated vapor pressures (Figures 1 and 2) show that the TraPPE-UA force field predicts carboxylic acid vapor pressures that are larger than the experimental values, which is consistent with the results obtained by Kamath et al.<sup>22</sup> This deviation from the experimental vapor pressures decreases with increasing temperature. According to Kamath and co-workers, this effect is directly related to the molecules aspect ratio  $L^* = L/\sigma$ , where  $L$  is the distance separating site centers and  $\sigma$  is the collision diameter.<sup>22,35</sup> Although options do exist for improving

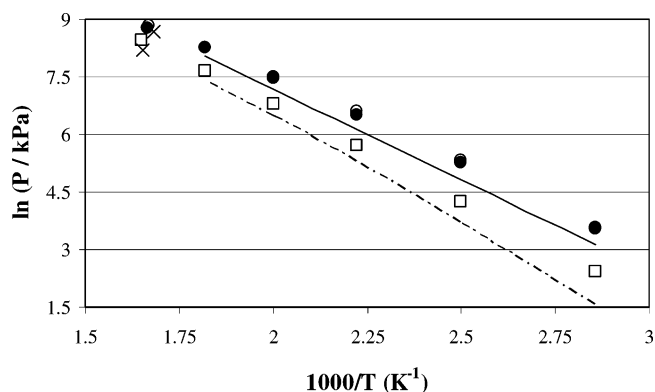


**Figure 1.** Clausius–Clapeyron plots of the saturated vapor pressure against inverse temperature for acetic acid and 2-methylpropanoic acid. Experimental data are represented as lines and simulation data as symbols: acetic acid, solid line and circles; 2-methylpropanoic acid, dashed line and squares. Filled symbols indicate data of Kamath et al.,<sup>22</sup> and the crosses represent the experimental critical points.

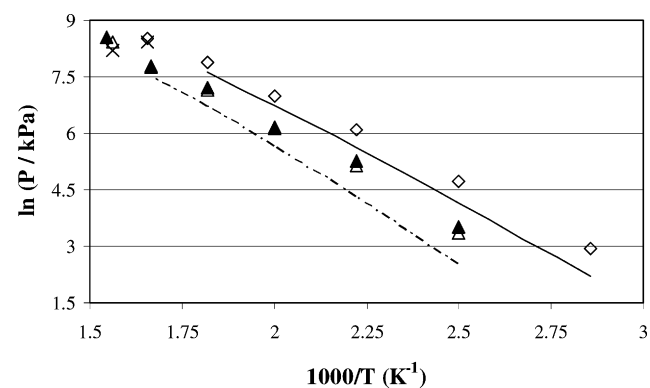


**Figure 2.** Clausius–Clapeyron plots of the saturated vapor pressure against inverse temperature for propanoic acid and pentanoic acid. Experimental data are represented as lines and simulation data as symbols: propanoic acid, solid line and diamonds; pentanoic acid, dashed line and triangles. Filled symbols indicate data of Kamath et al.,<sup>22</sup> and the crosses represent the experimental critical points.

the vapor pressure prediction through alteration of the aspect ratio,<sup>22</sup> the goal of the TraPPE-UA force field parametrization was to accurately represent the saturated liquid densities and critical temperature, which effectively fixes the simulated vapor pressures.<sup>22</sup>

As is observed in Figures 3 and 4, the saturated liquid densities are all in close agreement with experiment,<sup>36–38</sup> with average deviations of less than 1.1%. Experimental vapor densities are available only for acetic acid,<sup>36</sup> and again the simulation results agree well with experiment (see Figure 3). For propanoic acid, 2-methylpropanoic acid, and pentanoic acid, experimental saturated vapor densities are not available. Interestingly, the predicted critical densities (discussed below and shown in Figures 3 and 4) are all very close to the corresponding experimental values, indicating that the simulated vapor densities are probably accurate. However, without experimental data for comparison, it is impossible to be certain.

The critical properties are presented in Table 6 (and are shown in Figures 1–4), along with the corresponding experimental data<sup>36–38</sup> and (where applicable) the values obtained by Kamath et al.<sup>22</sup> The critical temperatures and densities were estimated from the simulated vapor–liquid coexistence data by fitting to the density scaling law and law of rectilinear diameters.<sup>39</sup> During the fitting procedure, the effect of different values for the scaling exponent,  $\beta$ , was investigated. The best fit was found for an exponent of 0.29, rather than a value (commonly used for

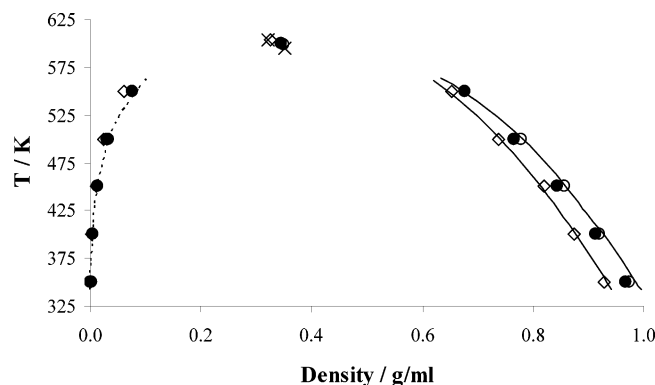


**Figure 3.** Vapor–liquid coexistence curves for acetic acid and propanoic acid. Experimental data are represented as lines (solid line for liquid density and dashed line for vapor density) and simulation data as symbols: acetic acid, circles; propanoic acid, diamonds. Filled symbols indicate data of Kamath et al.,<sup>22</sup> and the crosses represent the experimental critical points.

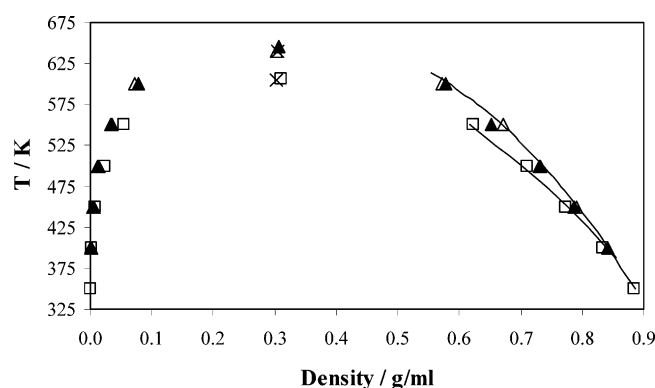


**Figure 4.** Vapor–liquid coexistence curves for 2-methylpropanoic acid and pentanoic acid. The experimental liquid densities are represented as solid lines and simulation data as symbols: 2-methylpropanoic acid, squares; pentanoic acid, triangles. Filled symbols indicate data of Kamath et al.,<sup>22</sup> and the crosses represent the experimental critical points.

alkanes) of 0.325. Interestingly, a similar result was found for alcohols by Chen et al.<sup>26</sup> This would indicate that for polar compounds (whose coexistence curves differ in shape from those of nonpolar species<sup>26</sup>), a lower value for the scaling exponent provides a better fit to the vapor–liquid coexistence data. The predicted critical temperatures and densities are all within 1% of experiment, except for 2-methylpropanoic acid where the density differed by approximately 2.5% (however, the simulated critical temperature for 2-methylpropanoic acid is 606.30 K, showing very good agreement with the experimental value of 605.0 K).

The predicted normal boiling points of the four acids, listed in Table 6, all lie below the experimental values (this is directly related to the overestimation of vapor pressures by the TraPPE-

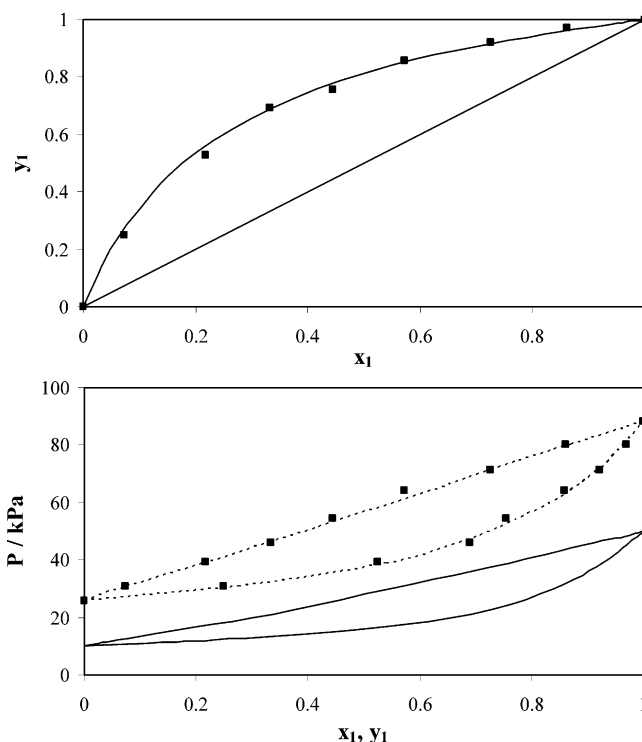


**Figure 5.**  $x$ – $y$  and  $P$ – $x$ – $y$  data for propanoic acid (1) and pentanoic acid (2) at 393.15 K. The solid lines represent the experimental data<sup>7</sup> and the filled squares the simulation results. The dashed line in the pressure–composition diagram is a guide for the eye.

UA model). However, the deviation from experiment was within 5% in all cases. Since the TraPPE-UA model predicts vapor pressures in excess of the experimental values, it also overpredicts the critical pressures, as shown in Table 6.

As discussed in section 2.1, to simulate 2-methylpropanoic acid using the TraPPE-UA force field, certain assumptions regarding bond angle and torsion parameters were required. Figures 1 and 4 and Tables 5 and 6 reveal that the 2-methylpropanoic acid simulations produced results indistinguishable in terms of accuracy from the results for the linear acids parametrized by Kamath et al.<sup>22</sup> This outcome demonstrates that the TraPPE-UA force field may be readily extended to include branched carboxylic acids.

**3.2. Binary Mixture Phase Behavior.** Simulation of binary VLE data for carboxylic acid systems has not previously been attempted. In this work, the TraPPE-UA force field has been used with the NPT Gibbs ensemble to simulate an isobar and an isotherm for two systems: propanoic acid + pentanoic acid and 2-methylpropanoic acid + pentanoic acid. These two systems were chosen since experimental data are available for comparison.<sup>7</sup> The simulation results are plotted in Figures 5–8 and are compared to the experimental data of Clifford et al.<sup>7</sup> For both systems, the simulated composition ( $x$ – $y$ ) diagrams

**TABLE 6: Critical Properties and Boiling Points**

compound	source	$T_c$ [K]	$\rho_c$ [g/mL]	$P_c$ [kPa]	$T_b$ [K]
acetic acid	experiment <sup>36</sup>	594.75	0.3512	5790	391.15
	Kamath et al. <sup>22</sup>	600.26	0.3444	6574	379.80
	this work	598.90	0.3492	6801	378.57
propanoic acid	experiment <sup>37,38,40</sup>	604.00	0.3221	4529	414.30
	this work	604.07	0.3256	5013	397.79
	experiment <sup>37,38,40</sup>	605.00	0.3017	3698	427.60
2-methylpropanoic acid	this work	606.30	0.3096	4761	412.09
	experiment <sup>37,38,40</sup>	639.90	0.3040	3629	459.30
	Kamath et al. <sup>22</sup>	646.40	0.3071	5230	435.70
pentanoic acid	this work	640.44	0.3036	4612	437.77



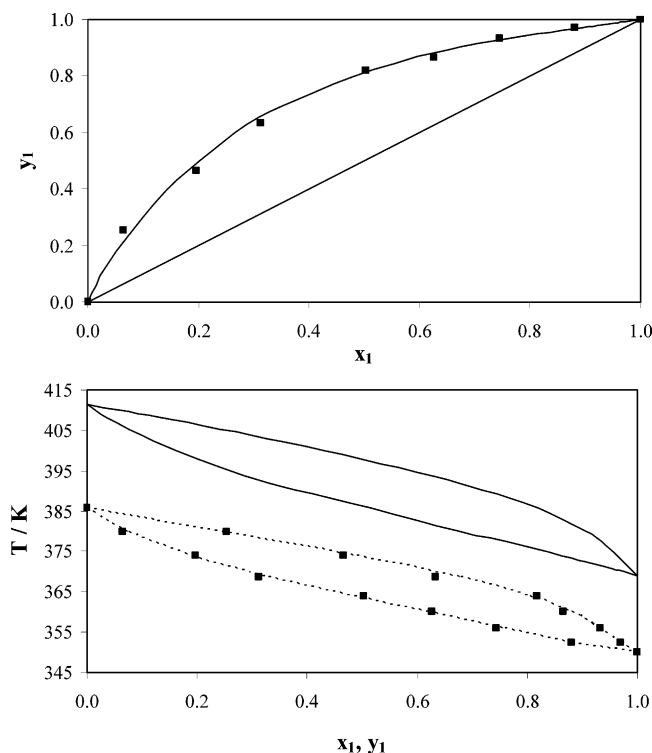


**Figure 6.**  $x$ - $y$  and  $T$ - $x$ - $y$  data for propanoic acid (1) and pentanoic acid (2) at 20 kPa. The solid lines represent the experimental data<sup>7</sup> and the filled squares the simulation results. The dashed line in the temperature-composition diagram is a guide for the eye.

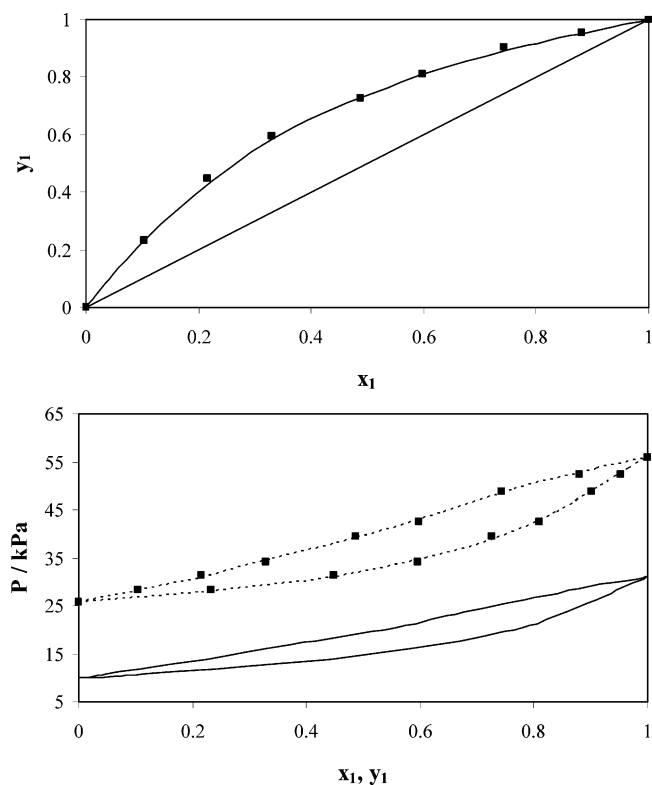


**Figure 7.**  $x$ - $y$  and  $P$ - $x$ - $y$  data for 2-methylpropanoic acid (1) and pentanoic acid (2) at 393.15 K. The solid lines represent the experimental data<sup>7</sup> and the filled squares the simulation results. The dashed line in the pressure-composition diagram is a guide for the eye.

are in close agreement with the measured experimental data (see Figures 5–8) and the  $P$ - $x$ - $y$  phase diagrams (Figures 5 and 7) and  $T$ - $x$ - $y$  diagrams (Figures 6 and 8) show the

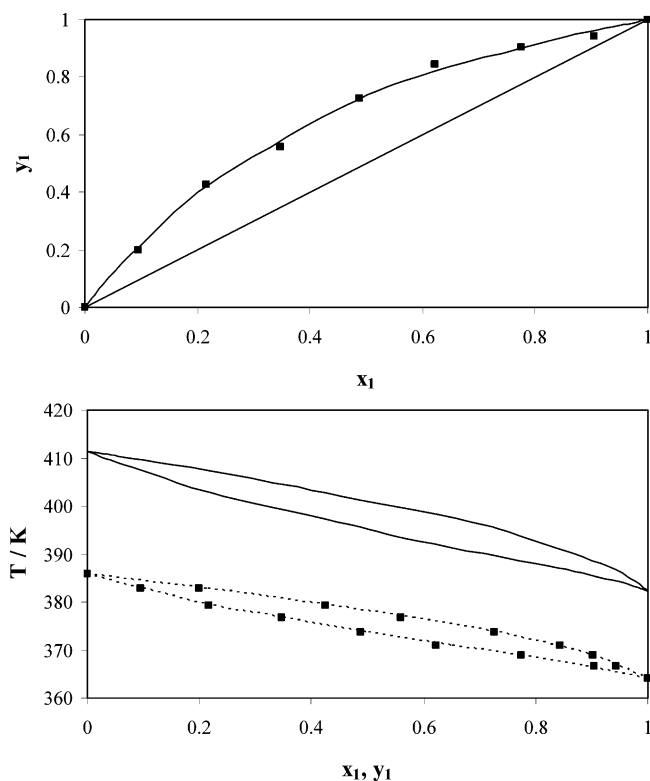


**Figure 8.**  $x$ - $y$  and  $T$ - $x$ - $y$  data for 2-methylpropanoic acid (1) and pentanoic acid (2) at 20 kPa. The solid lines represent the experimental data<sup>7</sup> and the filled squares the simulation results. The dashed line in the temperature-composition diagram is a guide for the eye.

anticipated pressure overprediction and temperature underprediction which come about as a direct consequence of the vapor pressure overestimation discussed in section 3.1. These deviations are within the expected range of 15–40 kPa and 20–30 K (for the isobars and isotherms, respectively), on the basis of the departure from experimental data observed for the pure component simulations. One of the consequences of this effect is the slight widening of the  $P$ - $x$ - $y$  phase envelopes and narrowing of the  $T$ - $x$ - $y$  phase envelopes evident in the simulation results.

#### 4. Conclusions

The simulated pure component carboxylic acid data are in good agreement with experimental data, although these systems are strongly associating. This includes the data obtained for the branched compound 2-methylpropanoic acid, where the angle and torsional parameters involving the  $-\text{CH}-$  pseudo-atom were assumed to be the same as those used for other functional groups in the TraPPE-UA force field. This indicates that this force field can be extended to branched carboxylic acids. The TraPPE-UA force field reproduces VLE data for binary carboxylic acid systems with an accuracy similar to that obtained for the pure component simulations. The  $x$ - $y$  data are in excellent agreement with experiment, while the  $P$ - $x$ - $y$  and  $T$ - $x$ - $y$  results show the expected discrepancy caused by the characteristic overprediction of the pure component saturated vapor pressures for the TraPPE-UA force field.

**Acknowledgment.** This work has been sponsored by the Swedish International Cooperation Development Agency (SIDA), SASOL, THRIP, the South African National Research Foundation Thuthuka Program, and the South African National Research Foundation International Science Liaison. We are

grateful to Peter Ahlström, University College of Borås, for valuable discussions.

## References and Notes

- (1) Grayson, M.; Eckroth, D.; Mark, H. F.; Othmer, D. F.; Overberger, C. G.; Seaborg, G. T. *Encyclopedia of Chemical Technology*, 3rd ed.; John Wiley & Sons: New York, 1978; Vol. 4.
- (2) Bruice, P. Y. *Organic Chemistry*, 2nd ed.; Prentice Hall: New Jersey, 1998.
- (3) Gerhartz, W.; Yamamoto, Y. S.; Campbell, F. T.; Pfefferkorn, R.; Rounsaville, J. F. *Ullmann's Encyclopedia of Industrial Chemistry*, 5th ed.; VCH: Weinheim, 1986; Vol. A5.
- (4) Codd, L. W.; Dijkhoff, K.; Fearon, J. H.; van Oss, C. J.; Roeberson, H. G.; Stanford, E. G. *Materials and Technology*; Longman-J. H. de Bussy: Amsterdam, 1972; Vol. 4.
- (5) Patai, S. *The Chemistry of Functional Groups Supplement B: The Chemistry of Acid Derivatives*, Part 1; John Wiley & Sons: Chichester, 1979.
- (6) Sewnarain, R.; Raal, J. D.; Ramjugernath, D. *J. Chem. Eng. Data* **2002**, *47*, 603–607.
- (7) Clifford, S. L.; Ramjugernath, D.; Raal, J. D. *Fluid Phase Equilib.* **2005**, *237*, 89–99.
- (8) Prausnitz, J. M.; Anderson, T. F.; Grens, E. A.; Eckert, C. A.; Hsieh, R.; O'Connell, J. P. *Computer Calculations for Multicomponent Vapour-Liquid and Liquid-Liquid Equilibria*; Prentice Hall: Englewood Cliffs, NJ, 1980.
- (9) Siepmann, J. I. *Mol. Phys.* **1990**, *70*, 1145–1158.
- (10) Mooij, G. C. A. M.; Frenkel, D.; Smit, B. *J. Phys.: Condens. Mater.* **1992**, *4*, L255–L259.
- (11) Frenkel, D.; Mooij, G. C. A. M.; Smit, B. *J. Phys.: Condens. Matter* **1992**, *4*, 3053–3076.
- (12) de Pablo, J. J.; Laso, M.; Suter, U. W. *J. Chem. Phys.* **1992**, *96*, 2395–2403.
- (13) de Pablo, J. J.; Laso, M.; Suter, U. W. *J. Chem. Phys.* **1992**, *96*, 6157–6161.
- (14) Laso, M.; de Pablo, J. J.; Suter, U. W. *J. Chem. Phys.* **1992**, *97*, 2817–2819.
- (15) Siepmann, J. I.; Frenkel, D. *Mol. Phys.* **1992**, *75*, 59–70.
- (16) Siepmann, J. I.; McDonald, I. R. *Mol. Phys.* **1992**, *75*, 255–259.
- (17) Smit, B.; Karaborni, S.; Siepmann, J. I. *J. Chem. Phys.* **1995**, *102*, 2126–2140.
- (18) Panagiotopoulos, A. Z. *Mol. Phys.* **1987**, *61*, 813–826.
- (19) Panagiotopoulos, A. Z.; Quirke, N.; Stapleton, M.; Tildesley, D. J. *Mol. Phys.* **1988**, *63*, 527–545.
- (20) Panagiotopoulos, A. Z. *Mol. Simul.* **1992**, *9*, 1–23.
- (21) Smit, B.; de Smedt, P.; Frenkel, D. *Mol. Phys.* **1989**, *68*, 931–950.
- (22) Kamath, G.; Cao, F.; Potoff, J. J. *J. Phys. Chem. B* **2004**, *108*, 14130–14136.
- (23) Panagiotopoulos, A. Z. *J. Phys.: Condens. Matter* **2000**, *12*, R25–R52.
- (24) Ungerer, P. *Oil Gas Sci. Technol.* **2003**, *58*, 271–297.
- (25) Martin, M. G.; Siepmann, J. I. *J. Phys. Chem. B* **1998**, *102*, 2569–2577.
- (26) Chen, B.; Potoff, J. J.; Siepmann, J. I. *J. Phys. Chem. B* **2001**, *105*, 3093–3104.
- (27) Potoff, J. J.; Siepmann, J. I. *AIChE J.* **2001**, *47*, 1676–1682.
- (28) Martin, M. G.; Chen, B.; Wick, C.; Stubbs, J. M.; Potoff, J. J.; Siepmann, J. I. *MCCCS-Towhee*, <http://www.cs.sandia.gov/projects/towhee/index.html>.
- (29) Martin, M. G.; Siepmann, J. I. *J. Phys. Chem. B* **1999**, *103*, 4508–4517.
- (30) Vlugt, T. J. H.; Martin, M. G.; Smit, B.; Siepmann, J. I.; Krishna, R. *Mol. Phys.* **1998**, *94*, 727–733.
- (31) Chen, B.; Siepmann, J. I. *J. Phys. Chem. B* **2000**, *104*, 8725–8734.
- (32) Allen, M. P.; Tildesley, D. J. *Computer Simulation of Liquids*, 1st ed.; Oxford University Press: Oxford, 1987.
- (33) Frenkel, D.; Smit, B. *Understanding Molecular Simulation from Algorithms to Applications*, 2nd ed.; Academic Press: San Diego, 2002.
- (34) McKnight, T. J.; Vlugt, T. J. H.; Ramjugernath, D.; Starzak, M.; Ahlström, P.; Bolton, K. *Fluid Phase Equilib.* **2005**, *232*, 136–148.
- (35) Stoll, J.; Vrabec, J.; Hasse, H.; Fischer, J. *Fluid Phase Equilib.* **2001**, *179*, 339–362.
- (36) Vargaftik, N. B. *Tables on the Thermophysical Properties of Liquids and Gases*, 2nd ed.; Hemisphere Publishing Corporation: Washington, 1975.
- (37) Daubert, T. E.; Danner, R. P. *Physical and Thermodynamic Properties of Pure Chemicals*; DIPPR, AIChE: New York, 1989.
- (38) Dortmund Data Bank Vapour-Liquid Equilibrium Data Compilation; DDBST GmbH: Oldenburg, 1973.
- (39) Rowlinson, J. S.; Swinton, F. L. *Liquids and Liquid Mixtures*, 3rd ed.; Butterworth: London, 1982.
- (40) Lide, D. R. *CRC Handbook of Chemistry and Physics*, 86th ed.; CRC Press: Boca Raton, FL, 2005.